Computational Study for Analysis of the Potential for Drag Reduction for Flow around a Circular Cylinder and Cactus-Shaped Cylinders

Magesh Raj Ravindran[1]

[1]Department of Aeronautical and Aerospace Engineering, Gurukul Vidyapeeth Institute of Engineering and Technology (GVIET),India

Abstract: *In the present paper, computational investigations of drag reduction on a smooth circular cylinder and cactus-shaped cylinders have been performed. The numerical study was performed using commercial CFD software Star CCM+ solving the Reynolds Averaged Navier-Stokes (RANS) equations at a Reynolds number of 140000. The k-ω model was tested. At first, the simulations were run for two-dimensional (2-D) smooth circular cylinders where three different domain sizes and eighteen different meshes for each domain size were considered. Therefore, 18 simulations were run for each domain size i.e. 54 simulations in total for the smooth circular cylinder. After analyzing the results obtained a suitable and best domain size and mesh were selected to further progress with the analysis of two-dimensional cactus shaped cylinder. For the analysis of cactus shaped cylinder, 20 variants i.e. 20 simulations of cactus geometry were investigated with 4 different numbers of peaks and 5 different numbers of amplitudes. Finally, the computational results obtained for drag coefficients, mean pressure distribution, mean stream wise velocity distribution and also the Strouhal frequency of vortex shedding were validated against experimental data. For cactus-shaped cylinders, results obtained for 20 peaks/bumps and 8 amplitudes showed reduction in drag, the surface pressure had better recovery, the wake turbulent velocity was lower, the Strouhal numbers were lesser and the mean stream wise velocity healed faster.*
Keywords:Amplitudes,Cactus-Shaped Cylinder, Drag Coefficient, Numerical Analysis, Peaks, Strouhal number.

I. INTRODUCTION

In the past few decades from 1930s, the development of accurate and effective numerical methods for the simulation of the flow around a cylinderhas been subject of intensive research activities in both the academic and industrial communities. Cylindrical structures are ubiquitous in industry and the flow around them has been studied for more detailed understanding of vortex shedding frequency and drag forces. Some examples are landing gears on aircraft, pylons for wind turbines or industrial chimney stacks. Most recently, the research is being focused more on modifying the shape and surface of the cylinder in order to reduce the negative consequences associated with vortex shedding in the wake and cylinder vibrations that can lead to reduction of drag. Vortex shedding is the unsteady oscillating flow that takes place when a fluid such as air or water flows past a blunt cylindrical body at certain velocities depending on the size and shape of the body. Flow process in the wake of a cylinder involves the formation and shedding alternately from one side to the other. This alternate formation and shedding of vortices also creates alternating forces which occurs more frequently as the velocity of the flow increases. These alternating low pressure vortices on the downstream side of the object will tend to move the object towards the low pressure zone where its speed is smaller than the upstream velocity. These repeated patterns of swirling vortices are caused by unsteady separation of flow of a fluid around blunt bodies. It is called Von Karman Vortex Street named after the engineer and fluid dynamicist, Theodore von Karman. This phenomenon is very important in engineering design.

Vortex shedding has been examined in a significant number of studies. There are two types of methods by which vortex shedding can be analyzed. Active flow control method which is experimental based on managing the boundary layer separation through control loops. Some different techniques are synthetic jets, plasma actuators etc. The other method is Passive control method and is based on modifying the surface properties of the cylinder such as changing the surface geometry, its roughness, etc. which is considered for this computational research. Vortex shedding is considered to be a challenging area of fluid dynamics and it continues to present problems to designers in a number of key industrial areas, because it can lead to severe resonance (structural vibrations) of the structure. If the vortex shedding frequency is close to the structural vibration frequency of the structure, then the structure begins to resonate due to large fluctuating pressure forces. This will allow the structure's movement to become self-sustaining and will eventually lead to the destruction of the structure.

Cactus trees are tall and thick cylindrical plants which have U-shaped surface grooves protruding out of the plant. It was suggested by Talley et al. [1] that these U-shaped grooves can help to modify vortex shedding frequency. The DNS computations done by Babu and Mahesha[2] on cactus geometry have shown reductions in drag and in Strouhal number for Reynolds number (Re) below 1000. This was due to the presence of stationary vertical structures within cactus grooves. Walther and Morgenthal[3] numerically studied the starting flow around a cactus cylinder and also found the presence of vertical structures within the surface grooves. It is also well known that drag on a cylinder decreases when the wake behind it changes from laminar to turbulent flow. Zdravkovich[4] suggested a method by adding an obstacle on the top or bottom around the bluff body to reduce drag by altering the flow field. S. Talley and G. Mungal[5] also noticed that cactus plants had strong resistance to wind forces due to the longitudinal grooves attached to it.

The experiments conducted before by Tombazis&Bearman [6], Bearman& Owen [7] and Owen et al. [8] showed that one of the main causes of drag, the vortex shedding was decreased or even suppressed if the flow separation lines behind the cylinder are forced to be wavy (sinuous). J.C. Owen et al, P.W. Bearman and A.A. Szewczyk[9] found that for cylinder with hemispherical bumps attached there was a considerable amount of decrease in drag by 25% which was similar to the results obtained for cylinder with helical grooves by Shan Huang [10]. As for the experiments conducted by Yamagishi Y. and Oki M. [11] on cylinders with different shape of grooves it was seen that drag coefficient for cylinder with triangular grooves decreases by 15% compared to cylinder with arc grooves. This was due to the geometry of triangular grooves being smaller than that of arc grooves. It was noted that by changing the shape of grooves can have more significant reduction in drag coefficients. For experiments on cylinders with different number of grooves by Yamagishi Y. and Oki M. [12] it was noticed that there is a sudden drop in drag coefficient for the cylinder with 32 grooves for low Reynolds number compared to 20 and 26 grooves. Out of the three cylinders with different number of grooves the circular cylinder with 32 grooves had the best result.

This type of study on cylinder with grooves has touched different domainssuch as the aeronautical industry where, the grooved walls are installed on the aircraft in order to reduce drag. The main objective of this research is to investigate the flow around a cylinder by modifying its surface i.e. by adding bumps. Finally, it can be concluded from these past experiments that a rough surface cylinder was found to have a lower drag coefficient than a smooth surface cylinder.

II. COMPUTATIONAL DETAILS

2.1 Geometry Modelling

The process starts with a two-dimensional (2-D) drawing of the geometry of smooth circular cylinder. The flow around a smooth cylinder was investigated in three different domains which were different from one another in their dimensions and the placement of cylinder within the domains. Fig.5summarizes the computational domain and the boundary conditions employed in this study.

The geometry of the cactus (Fig. 1) is defined by the generic equation 1 in the polar coordinate system:

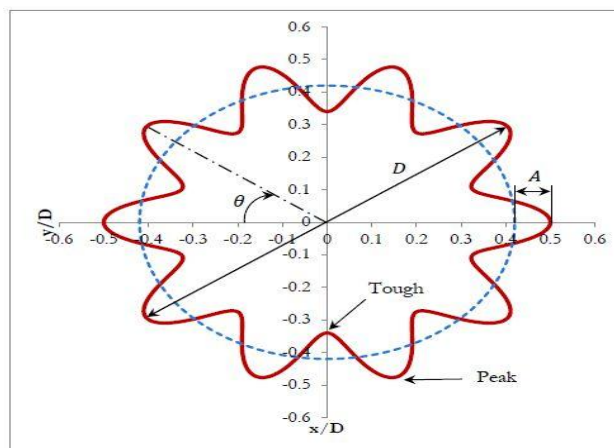Inner Radius + Amplitude × Cosine ((No. of Peaks) × Angle) $0^{\circ} \leqq \theta \leqq 360^{\circ}$ (1)

Fig. 1. Schematic of cactus-shaped cylinder cross-section

From Fig. 1, it should be noted that the angle, θ, starts from the leading edge and rotates along the clockwise direction.There were 20 variants of cactus geometry investigated in total which had four different peaks (10, 20, 30 and 40) and five different amplitudes (2, 4, 6, 8, and 10). These variants were sufficient to observe the effects of peaks and amplitudes on key flow parameters. Amplitude of sine wave is denoted by A and D is the diameter of the cactus. For the simulations, the cactus-shaped cylinder was also placed in the same position as that of smooth circular cylinder.

2.2 Grid generation (Meshing)

Accurate meshing of the domain is important as defining the physical models because an ill-conditioned mesh can give rise to very inaccurate results. The type of surface mesh used here was surface remesher. With this any region as per requirement gets meshed and it will help to refine the volume mesh. It can be used to fill holes, gaps etc. The type of volume mesh used was polyhedral mesh. It was specially chosen because it has several advantages compared to other types of meshes.The other type of mesh which was chosen near the wall of the cylinder was prism layer mesher. It tries to maintain a distance between vertices, not edges, so the prism layer will get smaller if there is a sharp convex angle which was noticed near the wall of cactus-shaped cylinders in which the number of peaks was kept more.

There were a total of 54 different types of meshes that were analyzed for smooth cylinder in which only the volume shapes and the refinement of volume mesh at certain regions was changed for three different domain sizes. There were only two major types of meshes with different volume shapes considered. The first one only had a block and the second was combined with four blocks and three cylinders. From these the second type of mesh with four blocks and three cylinders was chosen for the 20 simulations of cactus-shaped cylinder because it showed good results, in which only the geometry of the cactus differed. Three different shapes of blocks were considered for the simulations. Examples of some of the types of meshes generated for circular and cactus-shaped cylinder are shown below (Fig. 2-4). The common reference values or properties used for all the meshes are shown in Table 1.

Table 1. Mesh A and Mesh B properties

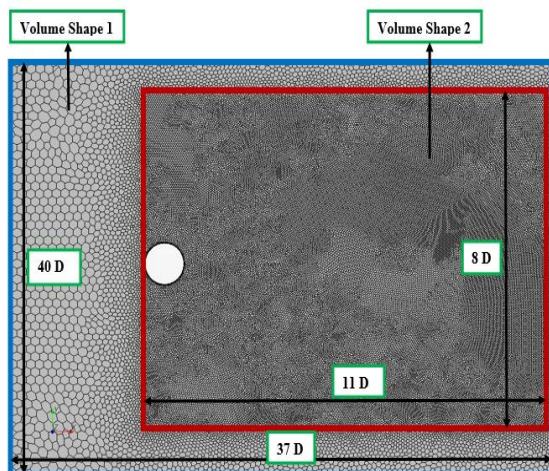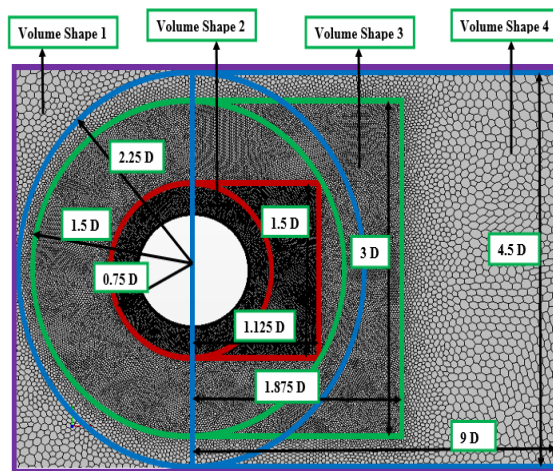|	
Number of Prism Layers	32
Prism Layer Thickness	0.025 m
Thickness of near wall Prism Layer	6.8E-5 m
Base Size	1 m
Surface Growth Rate	1.1
Growth Factor	0.85
Basic Surface Curvature	100 points/circle
Polyhedral Volume Blending Factor	0.5
Volume mesh 1 (for the whole domain)	0.25 m

Fig. 2. Smooth Circular Cylinder: Fig. 3. Smooth Circular Cylinder: Mesh B: Domain

Size: Mesh A: Domain Size: 37D × 40D,37D × 40D, Number of cells: 435612, Volume mesh 2: Number of cells: 136905, Volume mesh 2: 0.05 m0.01 m, Volume mesh 3: 0.02 m, Volume mesh 4: 0.08 m
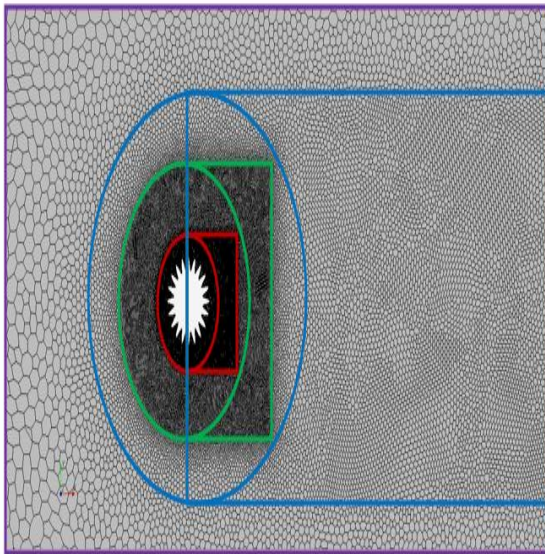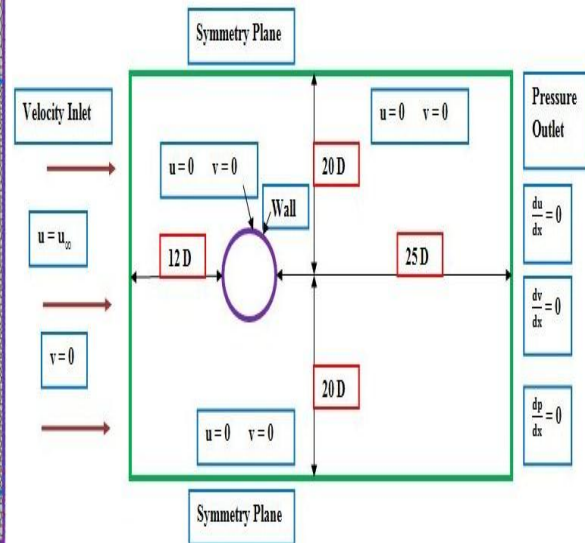

Fig. 4. Cactus Shaped Cylinder: Mesh B: Fig. 5. Schematic of boundary conditions for flow

Cactus 20 Peaks, 8 Amplitude: Domain Size: 37D × 40D,domain
Number of cells: 522432, Volume mesh 2: 0.01 m,
Volume mesh 3: 0.02 m, Volume mesh 4: 0.08 m

2.3 Define models and set properties
The turbulence model chosen was two-equation k-ω RANS model. The flow investigation was set to 2-D space. The material of the fluid was chosen liquid. As the flow Reynolds number is 140000, so the density (ρ), velocity (U_∞) was set to 1 and the kinematic viscosity was set to 7.142857×10^{-6}. Constant density was set for the equation of state. The turbulence intensity level which is defined by the ratio of fluctuating component of velocity to the mean velocity is set to 0.006 i.e. 0.6%.There are some relations (equations 2-5) which are necessary to solve before setting the parameters. As density (ρ) and kinematic viscosity (v) are fixed through the Reynolds number, the y^+ value can only be influenced through the normal wall distance y. So, the wall distance that ensures $y^+ < 1$ can be calculated as (the value of y^+ was reduced to 0.5):
The skin friction is calculated using the Schlicting skin-friction correlation:
$$C_f = [2.\log_{10}(Re_x) - 0.65]^{-2.3} \quad \text{for } Re_x < 10^9 \tag{2}$$
Therefore, $C_f = [2.\log_{10}(140000) - 0.65]^{-2.3} = 5.45 \times 10^{-3}$
The wall shear stress can then be determined:
$$\tau_w = C_f \times \frac{1}{2}.\rho U_\infty^2 \tag{3}$$
Therefore, $\tau_w = 5.45 \times 10^{-3} \times 0.5 \times 1 \times 1 = 2.725 \times 10^{-3}$ Pa
The friction velocity is thus determined as:
$$u_\tau = \sqrt{\frac{\tau_w}{\rho}} \tag{4}$$
So, $u_\tau = \sqrt{\frac{2.725 \times 10^{-3}}{1}} = 2.725 \times 10^{-3}$ ms⁻¹
The thickness of near wall prism layer can be computed as:
$$y = \frac{y^+ \times v}{u_\tau} \tag{5}$$
So, $y = \frac{0.5 \times 7.142857 \times 10^{-6}}{2.725 \times 10^{-3}} = 6.842 \times 10^{-5}$ m
2.4   Boundary conditions

It is very important to define all the inlet and outlet conditions and also the conditions on the walls and other boundaries of the domain which is a must. The flow angle was fixed to be parallel to the x-axis. Velocities were also fixed u = u_∞ and v = 0. No slip conditions were imposed on the cylinder for all the grid system. The domain used was split in to seven boundaries by angle which are shown in Fig. 5. For the upper and bottom symmetry plane the prism mesh was disabled to remove reflection of the flow from the wall. It was mainly done to save the number of cells as there was very little interference between the top and bottom cells. Neuman conditions were employed at the outer downstream boundary where the gradient of the dependent variables in the normal direction is fixed to zero.

2.5   Solver

For the solver the type of flow that was selected was segregated flow. Due to flow being unsteady around the cylinder in this case the time step chosen was implicit time stepping method. The computational time step is a very important parameter and it should be chosen carefully so that the physical phenomena required can be reproduced correctly. The time step chosen here is the minimum local time step over all fluid cells in the model. It is known that if the time step is large then it will lead to faster computational progress, but the time step is restricted by the Courant-Friedrichs-Lewy (CFL) condition.

In the software used Star CCM+, there exists a field function called Convective Courant Number which provides the local convective courant number for a given time step which was used to make sure that the CFL condition is satisfied. The local convective courant number is the ratio of physical time step to the mesh convection time scale. The discretization approach used was Finite Volume Method. The numerical scheme set was second order convection scheme. The convergence criteria were set through time step
.

III.   RESULTS AND DISCUSSIONS

3.1 Smooth circular cylinder

From the results it was found that domain 1 and mesh B shown before gave the best results. The domain sizes and dimensions of volume shapes with different mesh refinements used for the smooth circular cylinder investigations are shown in Table 2.Fig. 6 shows the contours of mean pressure coefficient and the mean stream wise velocity obtained for domain 1. Plots for mean pressure coefficient and mean stream wise velocity are shown in the validation section 3.1.1. The drag coefficient (C_D) found was 1.095422. The lift coefficient (C_L) was found to be negative i.e. -0.05903.

Table 2. Geometry of domain sizes, volume shapes and their mesh refinements

Mesh A Domain 1 (37D × 40D) Domain 2 (24D × 21D) Domain 3 (14D × 12D)	Block (Whole domain size)	Volume mesh 1 (0.25 m)
	Block (3D × 2D) Block (11D × 8D) Block (13D × 10D)	Volume mesh 2 (0.01 m, 0.05 m and 0.1 m)
Mesh B Domain 1 (37D × 40D) Domain 2 (24D × 21D) Domain 3 (14D × 12D)	Block (Whole domain size)	Volume mesh 1 (0.25 m)
	Block (1.125D × 1.5D) Cylinder radius (0.75 m)	Volume mesh 2 (0.01 m)
	Block (1.875D × 3D) Cylinder radius (1.5 m)	Volume mesh 3 (0.02 m)
	Block (9D × 4.5D) Cylinder radius (2.25 m)	Volume mesh 4 (0.08 m)

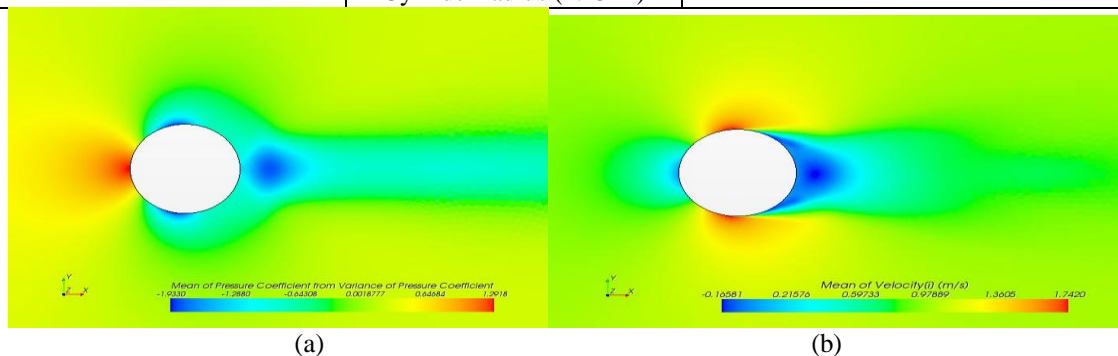(a)   (b)
Fig. 6. Contours of (a) Mean pressure coefficient (b) Mean stream wise velocity

From Fig. 6. (a), it can be seen that immediately adjacent to the surface of the cylinder a thin boundary layer (shown in blue color) is formed. This shows that there is no slip condition on the cylinder surface. It can also be noticed that the pressure is high (shown in red color) where the flow strikes the cylinder surface. At Reynolds number 140000, the boundary layer remains laminar from the stagnation point at the front of the cylinder to the point where it separates. After the flow passes the least pressure point, the flow experiences an adverse pressure gradient and separates as the pressure increases which is not clearly shown in the contour. Separation occurs because of excessive momentum loss near the wall of the cylinder in a boundary layer trying to move downstream and it decelerates the flow. Below the separation point, the flow speed in the reverse flow region is very high and it is close to the surface of the cylinder. The flow is reversed at the vicinity of the wall. This results in a second suction peak (drop of pressure coefficient) again on the surface of the cylinder. This shows the presence of local flow recirculation zone near the cylinder surface. Fig. 6. (b), shows that the velocity is minimum at the point where the flow strikes the cylinder surface and again increases upstream and downstream. As the flow passes behind the cylinder the velocity drops again rapidly. This variation in velocity shows the presence of stagnation point in the wake.

As discussed before that there is a field function called Convective Courant Number which is used to make sure that the CFL condition is satisfied i.e. the local convective courant number for a given time step should be less than 1. Fig. 7 shows the contour of convective courant number obtained for smooth circular cylinder. From the contour it can be seen that there is a symmetry formed behind the cylinder and also the convective courant number is much less than 1, i.e. around 0.37. Also the y^+ value plot obtained from the solution is shown in Fig. 8. From the plot it can be noticed that the y^+ value for smooth cylinder has not exceeded 0.5. The plot for Fast Fourier transform (FFT) is shown in Fig. 9. This plot helps to determine the Strouhal (St) number which is a parameter to find the vortex shedding frequency. As in this case it can be seen that the Strouhal number is around 0.2623 Hz.
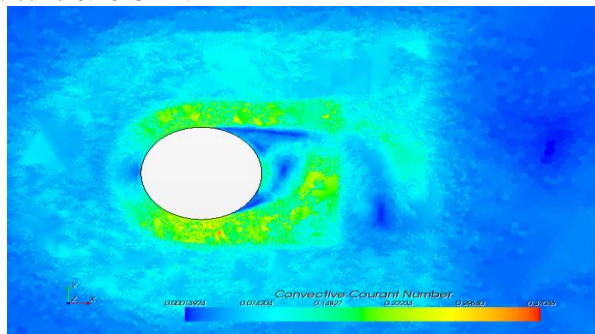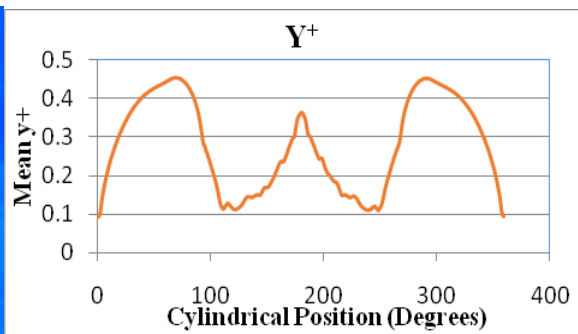

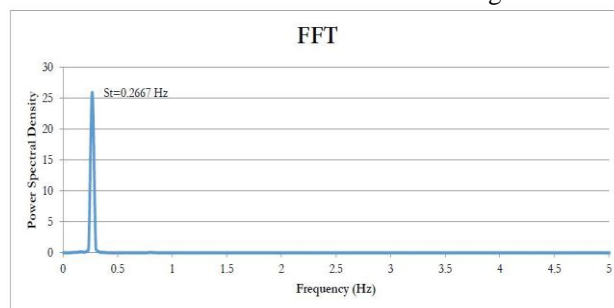Fig. 7. Convective courant number contour

Fig. 8. Time averaged y^+ value

Fig. 9. FFT plot using RANS model

3.1.1 Validation

After obtaining the results, validation was done for some of the main parameters with the past available experimental data of Cantwell and Coles. Cantwell and Coles [13] published a research paper in 1983 in which they experimentally measured various quantities of the flow in the first eight diameters of the wake around a circular cylinder using X-ray hot-wire probes at a Reynolds number of 140000. Here their findings will be used to validate the model. Fig. 10 shows time-averaged pressure distribution along the surface of smooth circular cylinder at Re = 140000. From the present study with RANS model (Fig. 10) it can be seen that there is a gradual drop in pressure coefficient. This is because in this case it takes time for the flow to move away from

the leading edge towards the wake which will lead to slow healing of the wake. It can also be seen that at the leading edge of the cylinder a stagnation point is formed which is brought to rest. Around both the sides of the cylinder, the flow accelerates around the forward surface producing a drop in pressure. Bernoulli's equation states that the pressure coefficient at the front stagnation point must have a value of 1.0. The present experimental study of Cantwell and Coles also agree on this.
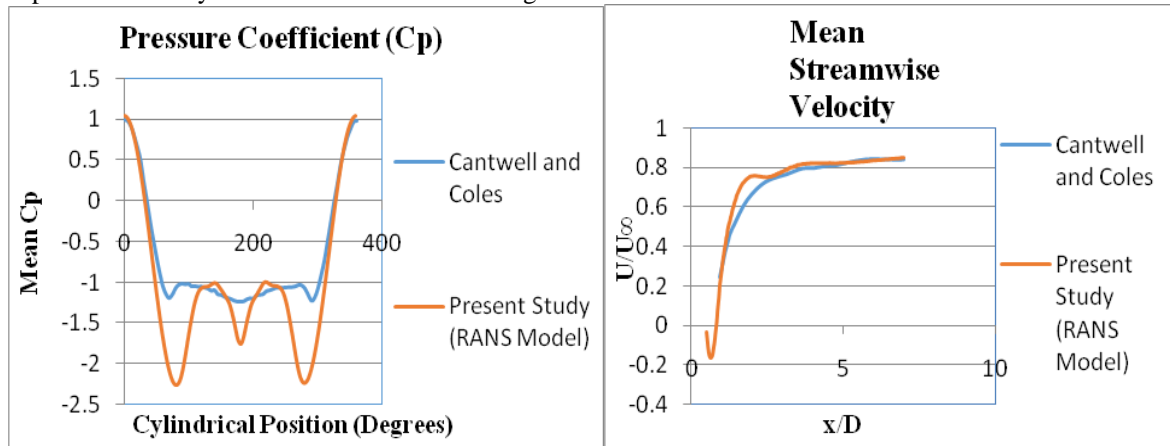

Fig. 10. Time-averaged pressure distribution   Fig. 11. Time-averaged mean stream wise velocity distribution

Again from Bernoulli's equation, there should be fall in pressure. Cantwell and Coles showed that the pressure reaches the trough at $70°$ which is $10°$ behind, i.e. it is $80°$ for the present study with RANS model has shown. From Cantwell and Coles data, it can also be seen from the curve that the pressure excursions are not arbitrarily large but they appear to be bounded above and below the envelopes that have the same general shape. It can also be observed that the lowest suction pressure coefficient i.e. the negative pressure is 45% less in the present study (RANS model) compared to the results presented by Cantwell and Coles. This difference between the results can be due to the choice of RANS model as one of its limitations when searched for states that the overproduction of turbulence through the over-prediction of turbulent kinetic energy and eventually turbulent viscosity in regions with large normal strain, such as stagnation regions and regions with strong acceleration. Fig. 11 shows the time-averaged mean stream wise velocity distribution at Re = 140000.

Fig. 11 shows qualitative comparison of streamlines obtained by averaging the instantaneous flow fields in time and in the span wise direction. It can be noted that U/U_∞ is the dimensionless stream wise velocity at the symmetry line y = 0. It can be seen from the figure that the results almost match with each other, especially the front and far wake regions. But still the present study (RANS) shows some oscillations in the results, maybe because the simulations were run for shorter time which can be remedied by running it for longer duration. Also, the present results have shown magnitude of reversed (negative) velocity with respect to the results of Cantwell and Coles. This can be due to the domain being too big and narrow that it accelerates the stream wise velocity. This is what happens in the middle wake region as the velocity considerably increases. The length of recirculation area is also underestimated by the simulation. The validated results of drag coefficient and Strouhal number are shown in Table 3.

Table 3. Validation of drag coefficient and strouhal number

Parameters	Cantwell and Coles	Present Study (RANS Model)
Drag Coefficient (C_D)	1.237	1.095
Strouhal Number (St)	0.179	0.262

In this flow regime around the cylinder the pressure drag was more dominant. This was due to the net imbalance of the pressure forces on the cylinder. Here, skin friction drag was also produced on the forward face of the cylinder where the velocity gradients were large and the boundary layer was thin. The total drag coefficient (C_D) of the present study (RANS model) was found to be reasonably close (11.47%) to that of provided by Cantwell and Coles (Table 3). The Strouhal number (St) obtained from the simulation is about 0.262 (Fig. 9) which is about 46.36% greater than that of presented by Cantwell and Coles i.e. 0.179. As

expected, the RANS computations of the sub-critical flow past the circular cylinder at Re = 140000 exhibits well known Von Karman Vortex Street with periodic vortex shedding.

3.2 Cactus shaped cylinder

The domain size and dimensions of volume shapes with different mesh refinements used for cactus-shaped cylinder investigations are shown in Table 4. Thecactus variants covered four different numbers of peaks (10, 20, 30 and 40) and five different numbers of amplitudes (2, 4, 6, 8 and 10). Selected cactus geometries defining equations in the polar coordinate system are given in Table 5. The mean pressure coefficient and stream wise velocity distribution contours of selectedcactus-shaped cylinders are shown in Table 6.
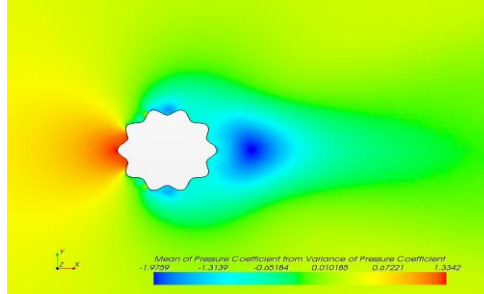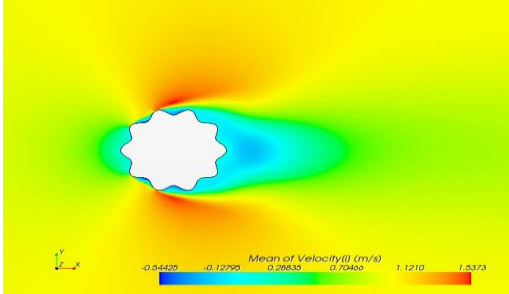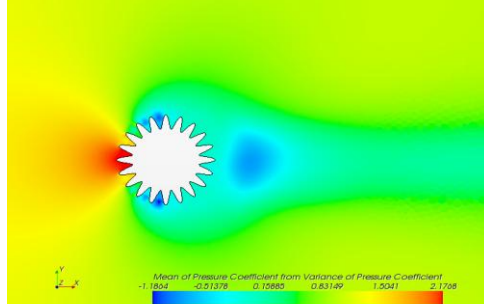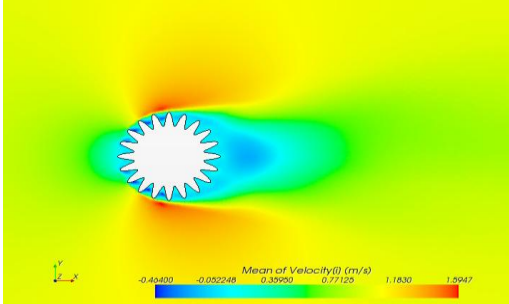
Table 4. Geometry of domain size, volume shapes and their mesh refinements

Mesh B Domain 1 (37D × 40D)	Block (Whole domain size)	Volume mesh 1 (0.25 m)
	Block (1.125D × 1.5D) Cylinder radius (0.75 m)	Volume mesh 2 (0.01 m)
	Block (1.875D × 3D) Cylinder radius (1.5 m)	Volume mesh 3 (0.02 m)
	Block (9D × 4.5D) Cylinder radius (2.25 m)	Volume mesh 4 (0.08 m)

Table 5. Defining equations for cactus geometries in polar coordinate system

Cactus 10 Peaks 4 Amplitudes	$0.46 + 0.04 \times \cos(10 \times \theta)$	$0° \leq \theta \leq 360°$
Cactus 20 Peaks 8 Amplitudes	$0.42 + 0.08 \times \cos(20 \times \theta)$	$0° \leq \theta \leq 360°$
Cactus 30 Peaks 10 Amplitudes	$0.40 + 0.10 \times \cos(30 \times \theta)$	$0° \leq \theta \leq 360°$
Cactus 40 Peaks 6 Amplitudes	$0.44 + 0.06 \times \cos(40 \times \theta)$	$0° \leq \theta \leq 360°$

Table 6. Mean Pressure Coefficient and Mean Stream wise Velocity distribution contours comparisons

Type of Model	Mean Pressure Coefficient Contours	Mean Stream wise Velocity Contours
Cactus 10P 4A		
Cactus 20P 8A		

Cactus 30P 10A		
Cactus 40P 10A		
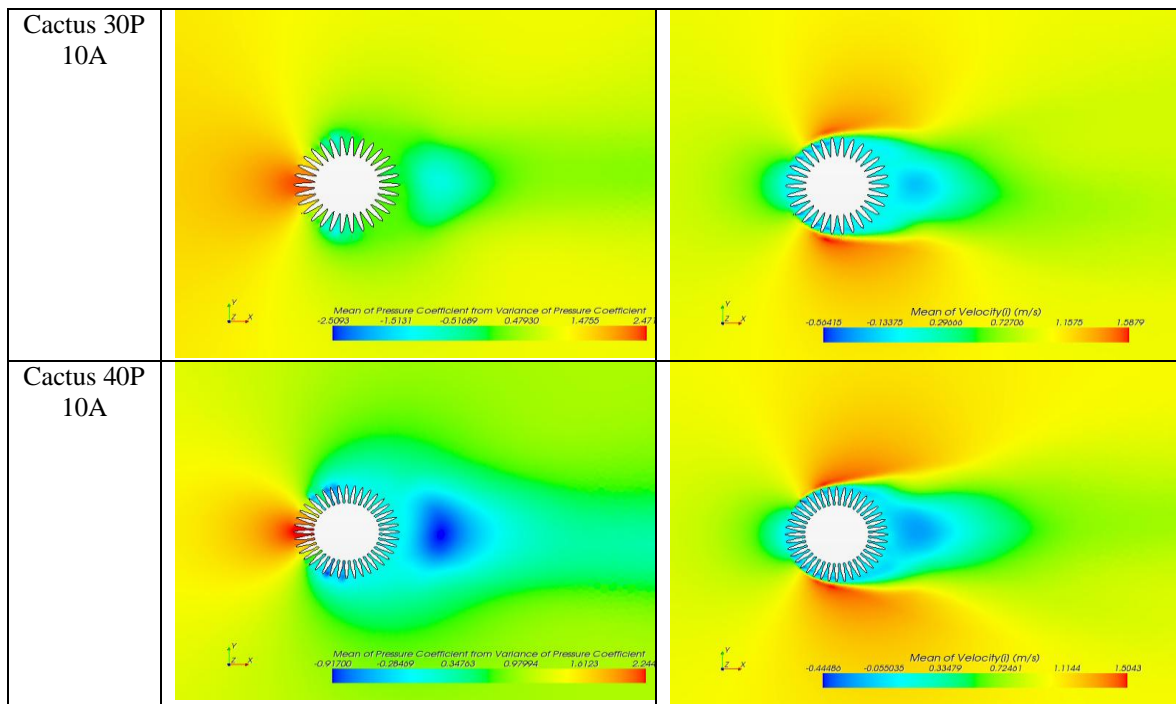
From the contours of mean pressure and velocity distributions shown in Table 6, it can be said that the overall trends of pressure coefficients for the two bluff-body geometries considered are similar, although there are certain differences. The pressure coefficient contour of smooth cylinder shows a smooth variation as there was no roughness present on the surface of the cylinder. But the contours of cactus-shaped cylinders show sharp spatial variations. The high pressure regions cover larger area in cacti than for smooth circular cylinder. The pressure coefficient for cactus-shaped cylinders drops much quickly and more steeply as the number of peaks are increased such as in case of Cactus 40P 10A, than for the smooth circular cylinder. The pressure coefficients are found to be lowest at the tip of the peaks and highest at the troughs where the flow strikes the cylinder. It was also observed that the flow separation is delayed for cactus-shaped cylinders than for smooth circular cylinder. As the number of peaks of the cactus increases there is a greater amount of recovery in pressure (i.e. base pressure is higher) which suggests a greater amount of decrease in drag as the number of peaks are increased. For the effect of amplitudes of the peaks on pressure recovery it can also be noticed for the case of cylinder with 20 and 30 peaks that as the number of amplitudes is increased, it considerably leads to decrease in pressure. But for the cacti with 10 and 40 peaks tend to have a little effect. Out of all the cacti cases investigated, it was noticed that the drag coefficient was more for the cacti with 10 peaks and gradually decreased with increase in number of peaks and amplitudes i.e. until the cylinder with 40 peaks. The least drag coefficient was found to be of Cactus 20P 8A. This shows that drag coefficient can definitely be reduced if an optimum choice of number of peaks and amplitudes are made.

It was also observed that the orientation of cactus had very little influence on the pressure distribution. It was noticed in some cases that when the peaks were facing the flow, there were greater negative pressures on the sides of the cacti leading to recovery of pressure which in turn increased the drag by a little amount. The mean stream wise velocity contours show similar velocity distributions in all cases, but the velocity is slightly higher for the cases of cacti compared to that of smooth circular cylinder. If the cylinder with 50 number of peaks was investigated, most probably the drag coefficient would have been increased due to increase in surface roughness of the cylinder.

3.2.1 Validation

After obtaining the results for cactus-shaped cylinder, validation was done with the experimental data of Abboud et al [14]. The mean pressure coefficient distribution plot (Fig. 12) of Cactus 10P 4A showed very close agreement out of all the results investigated but with some deviations with that of Abboud et al. The mean stream wise velocity distribution plot (Fig. 13) shows a little deviation, but as with the cylinder, the magnitude

of the reversed velocity is over predicted. All the simulations are found to be having considerable deviations. This might be due to the domain size being two narrow. It is important to note that the present study is done with Re = 140000, but Abboud et al. studied flows with Re = 210000 and with the geometry which was quite different, thus it is not expected that the results will match perfectly.
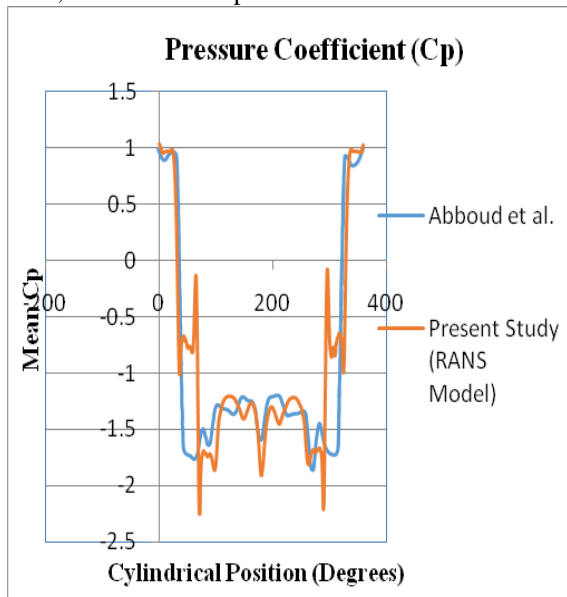

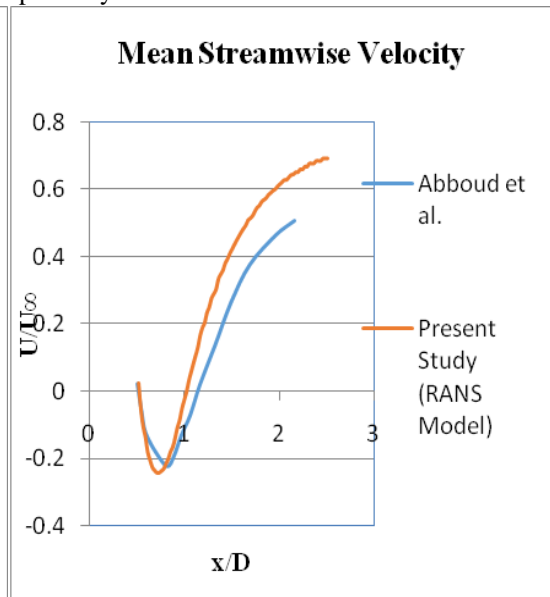Fig. 12. Time-averaged pressure coefficient distribution Cactus 10P 4A distribution for Cactus 10P 4A

Fig. 13. Time-averaged mean stream wise velocity for distribution for Cactus 10P 4A

The drag coefficient and vortex shedding frequency measurements of selectedcactus-shaped cylinders compared to that of smooth circular cylinder are shown in Table 7.

Table 7. Drag coefficient and vortex shedding frequency measurements comparisons

Type of Model	Drag Coefficient (C_D)	% difference of (C_D) to smooth cylinder	Strouhal Number (St)	% difference of (St) to smooth cylinder
Smooth Cylinder	1.095		0.262	
Cactus 10P 4A	1.3832	20.83 %	0.215	-21.86 %
Cactus 20P 8A	1.1612	5.7 %	0.239	-9.62 %
Cactus 30P 10A	1.219	10.17 %	0.249	-5.22 %
Cactus 40P 10A	1.229	10.9 %	0.249	-5.22 %

From Table 7 and also from Figure 14, it can be seen that the Strouhal number for the cactus-shaped cylinders are less than the smooth circular cylinder. This shows that the vortex shedding has been considerably reduced. The plots of FFT forselected cactus-shaped cylinders are shown in Figure 14.
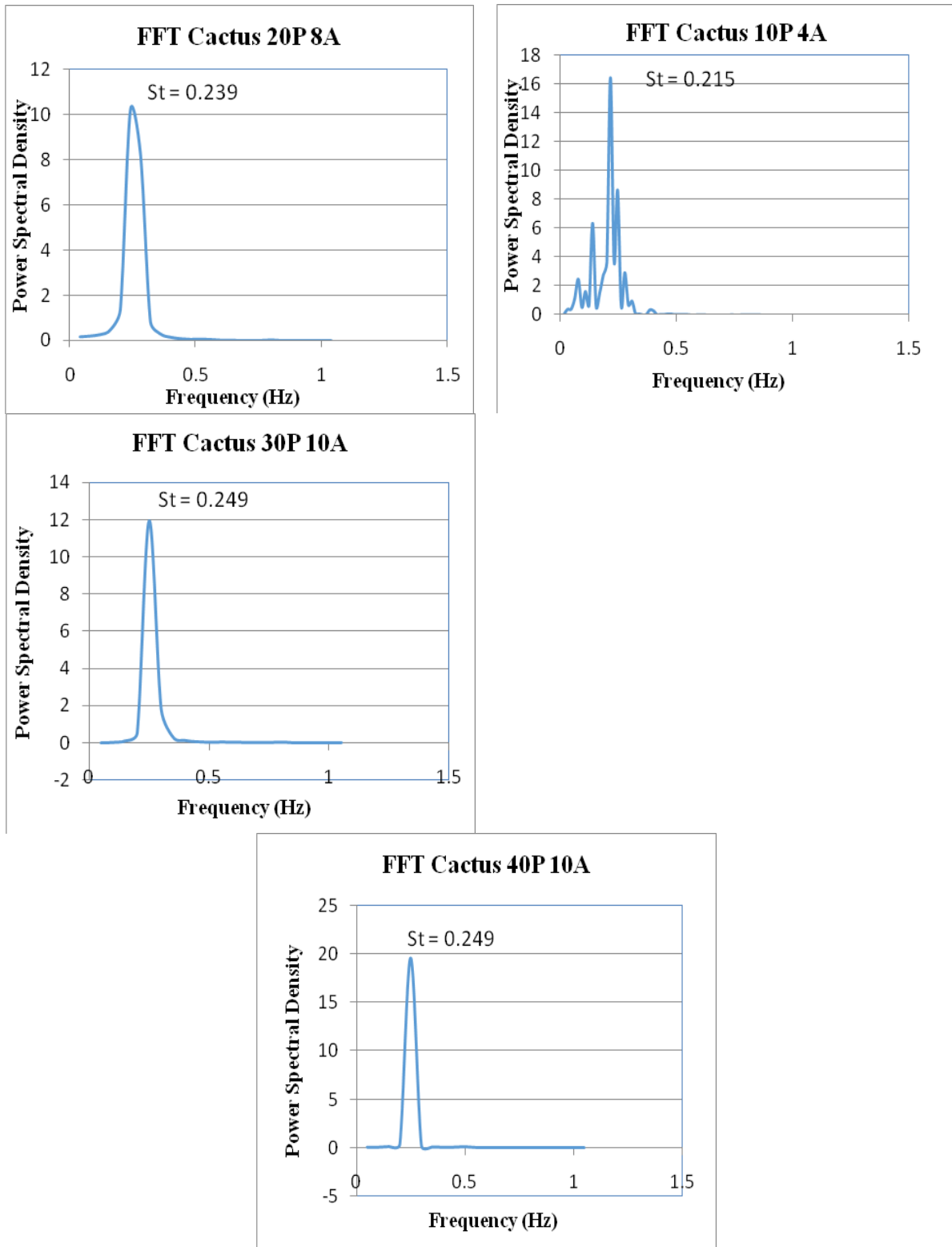
Fig. 14. FFT plots for selected cactus-shaped cylinders showing peaks of vortex shedding frequency (Strouhal Numbers)

IV. CONCLUSIONS

The investigation was carried out on smooth circular cylinder and cactus-shaped cylinders by changing the roughness of the surface of the cylinder i.e. in this case by adding bumps (peaks) on the surface of the cylinder. The Reynolds number considered for this research was 140000. Then the results obtained were validated with the experimental data.

From the 54 simulations for smooth circular cylinder, domain 1 and mesh B gave the best results which was validated with Cantwell and Coles experimental data as shown in the results section. The drag coefficient obtained was 1.095 which was found to be reasonably close (11.47 %) to the data provided by Cantwell and Coles. The convective courant number obtained was much less than 1. The Strouhal number obtained from the simulation for smooth circular cylinder was 0.262 which was 46.36 % greater than Cantwell and Coles data i.e. 0.179. The difference in the results validated was due to the domain being too narrow.

As domain 1 and mesh B showed good results for smooth cylinder simulations, the same was used for the 20 cactus-shaped cylinder simulations as well. 20 different variants of cactus geometry were considered in which the number of peaks and amplitudes differed. From the results, it was seen that increasing the number of peaks leads to decrease in significant amount of pressure. The results obtained were validated with Abboud et al. paper in which Reynolds number considered was 210000. The least drag coefficient was found for Cactus 20P 8A i.e. 20 peaks and 8 amplitudes. The cactus geometry that was used for the validation was Cactus 10P 4A which was found to be reasonably close to experimental data. The Strouhal numbers were less for cactus shaped cylinders i.e. there was a significant amount of decrease in vortex shedding which lead to drag reduction. The results hence confirmed that a significant amount of drag reduction can be obtained by making an optimum choice of number of peaks and amplitudes.

Future possible investigations might include more optimization of the mesh and can apply different turbulence model approaches at different Reynolds number. Future work can be carried out on 3-D model of cylinder. For cactus-shaped cylinders more work can be done by increasing the surface roughness i.e. by increasing the number of peaks and amplitudes.

REFERENCES

[1] Talley S, Iaccarino G, Mungal G, Mansour N. An Experimental and Computational Investigation of Flow Past Cacti. Center for Turbulence Research. 2001.
[2] Babu P, Mahesha K. Aerodynamic Loads on Cactus-Shaped Cylinders at Low Reynolds Numbers. Phys Fluids, 20. 2008;: p. 035112.
[3] Walther, J. H., and Morgenthal, G., 2002, "An Immersed Interface Method for the Vortex-in-Cell Algorithm," J. Turbulence, 3, pp. 1-9.
[4] Zdravkovich MM. Review of low interference between two circular cylinders in various arrangements. Trans ASME Fluids Eng. 99. 1977;: p. 618-633.
[5] Talley S, Mungal G. Flow around cactus-shaped cylinders.. Center for Turbulence Research Annual Research Briefs. 2002.
[6] Tombazis N, Bearman PW. A study of three-dimensional aspects of vortex shedding from a bluff body with a mild geometric disturbance. Fluid Mechanics 330. 1997;: p. 85-112.
[7] Bearman PW, Owen JC. Reduction of bluff-body drag and suppression of vortex shedding by the introduction of wavy separation lines. Fluids and Structures 12. 1998;: p. 123-130.
[8] Owen JC, Szewczyk AA, Bearman PW. Suppressing Karman vortex shedding by use of sinuous circular cylinders. Bulletin of the American Physical Society 44. 1999;: p. 124.
[9] Owen, J. C., Bearman, P.W., and Szewczyk, A. A., 2001, "Passive Control of VIV With Drag Reduction," J. Fluids and Structures, 15, pp. 597-605.
[10] Huang S. Drag reduction of deepwater risers by the use of helical grooves. In International Conference on Offshore Mechanics & Arctic Engineering; 2007; San Diego.
[11] Yamagishi, Y., and Oki, M., 2004, "Effect of Groove Shape on Flow Characteristics around a Circular Cylinder with Grooves," J. Visualization, 7(3), pp. 209-216.
[12] Yamagishi, Y., and Oki, M., 2005, "Effect of the Number of Grooves on Flow Characteristics around a Circular Cylinder with Triangular Grooves," J. Visualization, 8(1), pp. 57-64.
[13] Cantwell and Coles, Journal of Fluid Mechanics, An experimental study of entrainment and transport in the turbulent near wake of a circular cylinder, 1983, 321-374
[14] Abboud, J. E., Karaki, W. S., and Oweis, G. F., 2011, "Particle Image Velocimetry Measurements in the Wake of a Cactus-Shaped Cylinder," J. Fluids Engineering, 133, pp. 1-3.